



PAMAM dendrimers functionalized with ruthenium nitrosyl as nitric oxide carriers



Antonio Carlos Roveda Jr.^a, Thiago Bueno Ruiz Papa^a, Eduardo Ernesto Castellano^b, Douglas Wagner Franco^{a,*}

^aInstituto de Química de São Carlos, Universidade de São Paulo, Av. Trabalhador São-carlense, n° 400, 13566-590 São Carlos, SP, Brazil

^bInstituto de Física de São Carlos, Universidade de São Paulo, Av. Trabalhador São-carlense, n° 400, 13566-590 São Carlos, SP, Brazil

ARTICLE INFO

Article history:

Available online 11 July 2013

Metallodendrimers Special Issue

Keywords:

PAMAM dendrimer
Functionalization
Ruthenium nitrosyl complexes
Nitric oxide release
NO-donor

ABSTRACT

The functionalization of three generations of polyamidoamine (PAMAM G0, G2 and G3) dendrimers with the NO-donor *trans*-[Ru(NO)(NH₃)₄(ina)](BF₄)₃ (ina = isonicotinic acid) is reported. PAMAMs were modified through a peptide-type bond between the carboxyl group of the *ina* ligand and the dendrimer superficial amines. Compounds were characterized by FT-IR, UV-Vis, CV, DPV, ¹H NMR, ICP-OES, and the structure of the complex *trans*-[Ru(NO)(NH₃)₄(ina)](BF₄)(SiF₆)·H₂O was determined by single crystal X-Ray analysis. The experimental data indicated the immobilization of 4, ~8 and ~27 nitrosyl complexes on the G0, G2 and G3 dendrimer's surface, respectively, which corresponds to ~1.0–1.43 μmol NO per mg of dendrimer. FT-IR, UV-Vis and electrochemical assays suggest that the functionalization of PAMAM did not alter the coordination sphere of the ruthenium nitrosyl complex neither the formal reduction potential of Ru^{II}NO⁺/Ru^INO⁰ couple regarding to the complex not attached to PAMAM. The NO release in these compounds, through light irradiation (λ = 355 nm) and one-electron reduction (Eu²⁺), was investigated.

© 2013 Elsevier B.V. All rights reserved.

1. Introduction

The free radical nitric oxide (NO[•]) is an important signaling molecule [1,2], endogenously produced in the human body, which is associated with several biological functions [3]. The wide range of physiological and pathophysiological functions in which NO is involved, demands methods for storage and control the NO delivery at specific sites. Different compounds have been developed as effective NO donors, such as nitrosothiols, diazeniumdiolates, organic nitrates and nitrites, and also metal nitrosyl complexes [4,5]. These compounds are helpful to better understand the biological functions of NO and some of them exhibited potential therapeutic activities [6–11].

Among the different NO donors, ruthenium nitrosyl complexes of the type *trans*-[Ru(NO)(NH₃)₄(L)]³⁺ [12] are particularly attractive due to their water solubility, low toxicity to the host cells [7], stability in aqueous solution in the presence of oxygen [13] and robustness regarding substitution reactions [14]. The NO release in these compounds can be triggered either by one-electron reduction [12] or by light irradiation [15].

Similar to other NO donors, ruthenium nitrosyl complexes have been attached to different platforms aiming diverse purposes [16,17], such as the production of materials with a high NO payload [18], the controlled NO bioavailability at specific sites [19] and the improvement of NO donors stability [20]. Silica [21,22], xerogels [23–25], liposomes [26,27], nanoparticles [28] and dendrimers [18,29,30], are common examples of matrices that have been used as NO-releasing vehicles [17,31]. Dendrimers are attractive molecules for NO transport, once they can provide a scaffold for storing large amounts of NO on a single framework [18]. They also have a well defined branching structure with a multivalent surface, which can be useful for simultaneous interactions to multiple receptors [32,33]. These molecules have been extensively studied as drug delivery systems and imaging contrast [34–36]. Among the variety of dendrimers, Polyamidoamine (PAMAM) is a noteworthy class due to its water solubility and amine or carboxyl surface, which allows tailoring through different kinds of reactions with molecules or ions of interest [37–39].

Some dendrimers have already been synthesized aiming nitric oxide transport and release [18,19,29,30,20]. For example Stasko and Schoenfisch [18] synthesized polypropylenimine (PPI) dendrimers (G3 and G5) functionalized with *N*-diazeniumdiolates which were able to store ~5.6 μmol NO per mg of compound. Following a similar approach, Lu et al. [20] synthesized a series of amine PPI dendrimers (G2–G5) functionalized with different surface groups,

* Corresponding author. Tel.: +55 16 3373 9970; fax: +55 16 3373 9976.
E-mail address: douglas@iqsc.usp.br (D.W. Franco).

in which the NO storage capacity was in the range of 0.9–3.8 μmol NO per mg of compound [20]. Stasko and collaborators [29] also synthesized a G4 PAMAM functionalized with *S*-nitrosothiols which were able to store ~ 2 μmol NO per mg of compound. Benini and collaborators [30] functionalized PAMAM dendrimers (G0, G2 and G3) with the $[\text{Ru}(\text{edta})(\text{NO})]^-$ complex, which were capable of storing around 1.4–1.8 μmol NO per mg of compound.

In this context, this work reports the synthesis and characterization of the complex $\text{trans-}[\text{Ru}(\text{NO})(\text{NH}_3)_4(\text{ina})]^{3+}$ (ina = isonicotinic acid) attached to PAMAM dendrimers of generations 0, 2 and 3. Some reactivity aspects of these compounds regarding NO release are also discussed. The *ina* ligand was chosen because it provides a carboxyl group for the attachment to PAMAM's superficial amines. Furthermore, after the amide bond formation, the structure of the complex $\text{trans-}[\text{Ru}(\text{NO})(\text{NH}_3)_4(\text{ina})]^{3+}$ attached to the dendrimer becomes similar to the structure of $\text{trans-}[\text{Ru}(\text{NO})(\text{NH}_3)_4(\text{isn})]^{3+}$ (isn = isonicotinamide), which exhibited the best results among the complexes of type $\text{trans-}[\text{Ru}(\text{NO})(\text{NH}_3)_4(\text{L})]^{3+}$ in tests against Chaga's disease [7,8].

2. Experimental section

2.1. Chemicals and reagents

The analytical grade reagents (Aldrich or Merck) and solvents (Mallincrodt, Baker, Merck or Panreac) were used as purchased, except PAMAM dendrimers (20 wt.% in methanol), which were dried under vacuum to remove methanol before using. Ruthenium trichloride ($\text{RuCl}_3 \cdot x\text{H}_2\text{O}$) was the starting reagent for the synthesis of all the complexes described herein. The synthesis and manipulations were performed under an argon atmosphere using standard techniques [40]. Eu^{2+} solution was prepared by adding Eu_2O_3 (99.99%) in a deaerated acid solution (0.10 mol L^{-1} trifluoroacetic acid) containing Zn(Hg). The reduction of Eu^{3+} to Eu^{2+} was completed after 40 min, and then the solution was used immediately. Deionized water (Millipore) was used throughout this work.

2.2. Instruments

Electronic spectra were recorded in a Hitachi U-3501 or Agilent 8453 UV–Vis spectrophotometer model using a 1.00 cm quartz cell. The solid-state infrared measurements were recorded in a Bomem MB 102 FTIR spectrophotometer using KBr pellets, 128 scans and resolution of 4 cm^{-1} in the 4000–400 cm^{-1} range. The FTIR measurements for PAMAM (oil) were performed in a silicon window using the same conditions described before for the assays using KBr pellets. The elemental analyses were performed on a Perkin–Elmer CHN 2400. Ruthenium analysis was carried out using a Perkin Elmer Optima 3000 DV Induced Coupled-Plasma Optical Emission Spectrometer (ICP–OES). Cyclic voltammetry (CV) and differential pulse voltammetry (DPV) experiments were performed with a PAR model 264A Potentiostat. The three-electrode system, saturated calomel, glassy carbon and platinum wire, were used as reference, work and auxiliary electrodes respectively. The potential values were converted and reported as normal hydrogen electrode (NHE). ^1H NMR spectra were recorded in a Bruker DRX 400 spectrometer using a trifluoroacetic acid-*d* solution (CF_3COOD , 1 mol L^{-1}) in D_2O . 3-(Trimethylsilyl)propionic-2,2,3,3-*d*₄ acid sodium salt was used as internal reference. Electron paramagnetic resonance (EPR) spectra were obtained in a Bruker EMX Plus X-band spectrometer at room or liquid nitrogen temperature. Samples were irradiated with a Nd:YAG LASER (Continuum, model Surelite-II) operating in the third harmonic ($\lambda = 355$ nm). A power meter (Coherent, Lasermate-P) measured the average energy per pulse.

2.3. Measurements

All experiments were carried out at 25 ± 1 $^\circ\text{C}$ in a phosphate buffer pH 7.4 (0.10 mol L^{-1} , $\mu = 0.20$ mol L^{-1} , or in aqueous solution pH 2.0, $\mu = 0.10$ mol L^{-1} ($\text{CF}_3\text{COOH}/\text{CF}_3\text{COONa}$). All manipulations were performed in the absence of oxygen. The inert gas (argon with high purity 99.998%) was deoxygenated by passing through a Cr(II) solution prior to use [40]. The nitrogen gas (99.999% of purity) was used without further purification. The complexes were stored under vacuum and protected from light and moisture. For ruthenium analysis, a calibration curve was prepared using a commercial standard ruthenium solution (1000 mg/L of Ru in HNO_3 2% water solution). The samples were prepared dissolving the ruthenium complexes in a trifluoroacetic acid solution (1.0×10^{-3} mol L^{-1}) and aliquots were taken for the analysis (ICP–OES). NMR, EPR and UV–Vis spectra of the solutions containing air-sensitive complexes were obtained under argon atmosphere. Solutions were transferred through Teflon tubing to specific cell or tube using the inert gas pressure.

2.4. Synthesis of $\text{trans-}[\text{Ru}(\text{NO})(\text{NH}_3)_4(\text{ina})](\text{BF}_4)_3$

The complexes $\text{trans-}[\text{Ru}(\text{NH}_3)_4(\text{ina})(\text{SO}_4)]\text{Cl}$ [41] and $\text{trans-}[\text{Ru}(\text{NO})(\text{NH}_3)_4(\text{ina})](\text{BF}_4)_3$ were synthesized and characterized as described in the literature [13,14]. Theoretical elemental analysis for $\text{trans-}[\text{Ru}(\text{NH}_3)_4(\text{ina})(\text{SO}_4)]\text{Cl} \cdot 2\text{H}_2\text{O}$: C, 15.67; H, 4.60; N, 15.23. Experimental elemental analysis: C, 15.90; H, 4.68; N, 14.92. Yield: 65–70%. Theoretical elemental analysis for $\text{trans-}[\text{Ru}(\text{NO})(\text{NH}_3)_4(\text{ina})](\text{BF}_4)_3 \cdot 2\text{H}_2\text{O}$: C, 11.65; H, 3.42; N, 13.58. Experimental elemental analysis: C, 11.51; H, 3.52; N, 13.43. Yield: 55–60%.

2.5. X-ray data collection and structure determination

Crystals of $\text{trans-}[\text{Ru}(\text{NO})(\text{NH}_3)_4(\text{ina})](\text{BF}_4)(\text{SiF}_6) \cdot \text{H}_2\text{O}$ were obtained from an aqueous solution (4.0 mol L^{-1} of HBF_4) of $\text{trans-}[\text{Ru}(\text{NO})(\text{NH}_3)_4(\text{ina})]^{3+}$ maintained at ~ 10 $^\circ\text{C}$ for one week. The presence of SiF_6^{2-} as counterion in the crystals was originated from the reagent HBF_4 , which contains SiF_6^{2-} as impurity ($\sim 0.2\%$), as previously reported [13]. The presence of SiF_6^{2-} as counterion in the crystals was also identified by FT-IR measurements through the bands at 740 and 480 cm^{-1} [42], which are absent in the amorphous solid $\text{trans-}[\text{Ru}(\text{NO})(\text{NH}_3)_4(\text{ina})](\text{BF}_4)_3 \cdot 2\text{H}_2\text{O}$. The band at 1080 cm^{-1} , assigned to BF_4^- anion [42], was also observed in the FT-IR for the complex $\text{trans-}[\text{Ru}(\text{NO})(\text{NH}_3)_4(\text{ina})](\text{BF}_4)(\text{SiF}_6) \cdot \text{H}_2\text{O}$. It is important to emphasize that the amorphous solid of $\text{trans-}[\text{Ru}(\text{NO})(\text{NH}_3)_4(\text{ina})]^{3+}$ has three BF_4^- as counterions, as confirmed by the FT-IR measurements and elemental analysis. Theoretical elemental analysis for $\text{trans-}[\text{Ru}(\text{NO})(\text{NH}_3)_4(\text{ina})](\text{BF}_4)(\text{SiF}_6) \cdot \text{H}_2\text{O}$: C, 12.66; H, 3.36; N, 14.76. Experimental elemental analysis: C, 12.41; H, 3.53; N, 14.56.

2.5.1. Crystal data

A yellow crystal of dimensions $0.163 \times 0.036 \times 0.026$ mm^3 was selected and mounted on an Enraf–Nonius Kappa-CCD diffractometer with graphite monochromated $\text{Mo K}\alpha$ ($\lambda = 0.71073$ Å) radiation. Data were collected at room temperature up to 52° in 2θ and final unit cell parameters were based on all reflections.

2.5.2. Data collection and processing

Data collections were made using the COLLECT program [43]; integration and scaling of the reflections were performed with the HKL Denzo–Scalepack system of programs [44]. Absorption corrections were carried out using the Gaussian method [45]. The structure was solved by direct methods with SHELXS-97 [46]. The model was refined by full-matrix least squares on F^2 by means of SHELXL-97 [47]. All hydrogen atoms were stereochemically positioned and

refined with the riding model except for the ones of the water molecule which were found from a difference map and refined with the O–H distance restrained to 0.82(2) Å. Fig. 1 was prepared using ORTEP-3 for Windows [48]. Listing of atomic coordinates and equivalent isotropic displacement parameters, full intramolecular bond distances and angles, hydrogen coordinates, and anisotropic thermal parameters are available from the authors and were deposited at the Cambridge Crystallographic Data Centre, reference numbers CCDC 929821. These data are also shown in Supplementary material (Tables 15–3S).

2.6. Functionalization of PAMAM dendrimers with *trans*-[Ru(NO)(NH₃)₄(ina)](BF₄)₃

Functionalization of PAMAM (G0, G2 and G3) with *trans*-[Ru(NO)(NH₃)₄(ina)](BF₄)₃ was performed via an amide bond formation using Yamaguchi reagent (2,4,6-trichlorobenzoyl chloride) [49–51]. Similar procedures were applied for the three PAMAM generations, as described below.

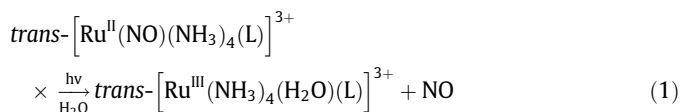
Under absence of air and moisture, a solution containing *trans*-[Ru(NO)(NH₃)₄(ina)](BF₄)₃ (75 mg, 0.121 mmol) in dry DMF (4 mL) was treated with triethylamine (Et₃N) (0.133 mmol, 20 μL) and 2,4,6-trichlorobenzoyl chloride (0.133 mmol, 22 μL). The resulting suspension was stirred at room temperature (25 °C) for ~24 h and then, 4-Dimethylaminopyridine (DMAP, 0.242 mmol) and PAMAM (0.080 mmol of superficial NH₂) dissolved in dry and degassed DMF (~5 mL) were added in sequence. The mixture was stirred at room temperature (25 °C) during 96 h for G0, 120 h for G2 and 168 h for G3. The resulting suspension was filtered and the solid was washed with DMF and dried under vacuum. The product was dissolved in ~2 mL of 2.0 mol L⁻¹ HBF₄ solution, which was filtered and the supernatant was purified by size exclusion chromatography (Sephadex G-25). The first fraction collected in the chromatographic column was evaporated (rotary evaporator) to a minimal volume (~3–4 mL), and then 1.0 mL of 5.0 mol L⁻¹ HBF₄ was added. After the addition of degassed ethanol (~15 mL), the solution was cooled in refrigerator and a precipitate was formed. These solids were collected by filtration, washed with

ethanol and dried under vacuum. The obtained products are described throughout this text for simplicity as G_x/RuNO (where *x* = 0, 2 or 3, and represents PAMAM generations). Ruthenium nitrosyl attached to PAMAM were hygroscopic, and this property increased with the increasing of the dendrimers generation. Yield = 40–45%.

2.7. Nitric oxide release

Nitric oxide release from ruthenium nitrosyl complexes (attached or not to PAMAM) was performed in solution through light irradiation and by one-electron reduction [12–15].

In the photochemical experiments, samples were irradiated ($\lambda_{\text{irr}} = 355 \text{ nm}$) with a Nd:YAG Laser, 10 ns pulse width, attenuated to approximately 2 mJ/pulse, in a 1.00 cm path length quartz cells capped with a rubber septum and under constant argon flow. The progress of the photoreaction, in aqueous solutions pH 2.0 ($\mu = 0.10 \text{ mol L}^{-1} \text{ CF}_3\text{COOH}/\text{CF}_3\text{COONa}$; $C_{\text{Ru}} \sim 9.0 \times 10^{-5} \text{ mol L}^{-1}$), was monitored spectrophotometrically (UV–Vis). Also, Ru³⁺, one of the photoproducts (Eq. (1)) [12,15], was detected through EPR spectroscopy after the light irradiations ($t_{\text{irr}} = 30 \text{ min}$) of aqueous solution of ruthenium nitrosyl complex ($C_{\text{Ru}} \sim 2.0 \times 10^{-3} \text{ mol L}^{-1}$, pH 2.0, $\mu = 0.10 \text{ mol L}^{-1} \text{ CF}_3\text{COOH}/\text{CF}_3\text{COONa}$).



The detection of the nitric oxide released from ruthenium nitrosyl complexes after light irradiation was performed through EPR spectroscopy, using the NO spin trap 2-phenyl-4,4,5,5-tetramethylimidazoline-1-oxyl-3-oxide (PTIO) [52,53]. Thus, a phosphate buffer solution (pH 7.4, 0.10 mol L⁻¹, $\mu = 0.20 \text{ mol L}^{-1}$) containing ruthenium complexes ($C_{\text{Ru}} = 7.5 \times 10^{-4} \text{ mol L}^{-1}$) and PTIO ($C_{\text{PTIO}} = 7.5 \times 10^{-4} \text{ mol L}^{-1}$) was irradiated for 5 min. A solution containing only PTIO was irradiated for 10 min, in the same conditions described above and was used as control.

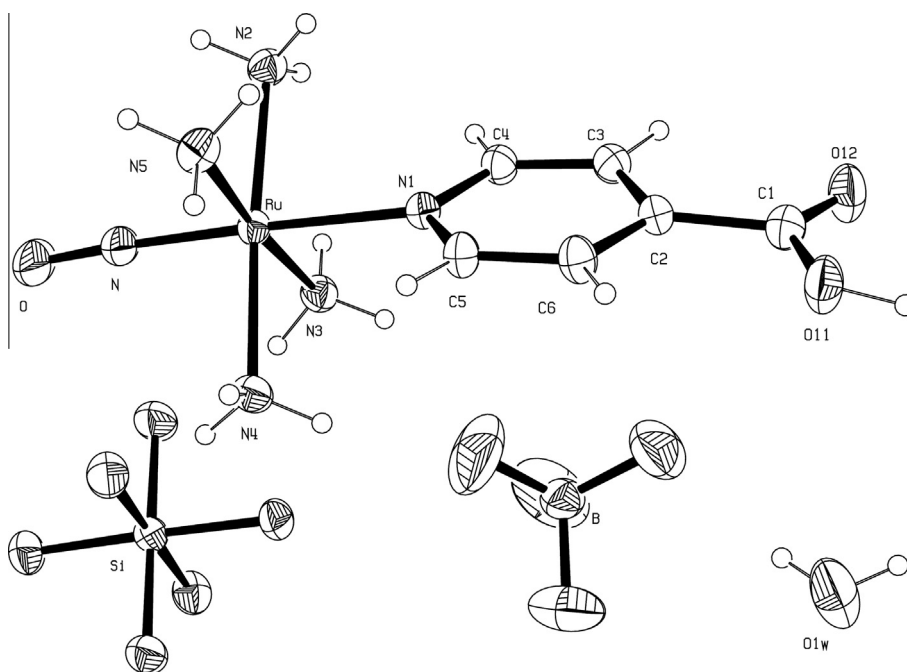


Fig. 1. ORTEP-3 structure representation for *trans*-[Ru(NO)(NH₃)₄(ina)](BF₄)(SiF₆)·H₂O with displacement ellipsoids displayed at 30% probability.

For the NO release from chemical reduction, *trans*-[Ru(NO)(NH₃)₄(ina)](BF₄)₃ (attached or not to PAMAM) was solubilized in degassed aqueous solution pH 2.0, $\mu = 0.10 \text{ mol L}^{-1}$ (CF₃-COOH/CF₃COONa) and then an excess of Eu²⁺ (4 equivalents) was added [13,14]. Differential pulse voltammetry (DPV) and electronic spectroscopy were used to help the detection and characterization of the produced species.

3. Results and discussion

3.1. Synthesis

The crystallographic data for *trans*-[Ru(NO)(NH₃)₄(ina)](BF₄)(SiF₆)-H₂O are listed in the Table 1, and the selected bond lengths and angles are shown in Table 2. Four NH₃ ligands occupy the equatorial positions and, *ina* and NO⁺ ligands are in *trans* position in the axial direction (Fig. 1). The mean of the Ru–NH₃ distance is $2.113 \pm 0.009 \text{ \AA}$ and the Ru–NO distance is 1.741(4). These both values are similar to those found for other nitrosylammineruthenium complexes such as [Ru(NH₃)₅(NO)]Cl₃ [54] and *trans*-[Ru(NO)(NH₃)₄(L)](X)_n (where L = N-heterocyclic and X = PF₆⁻, Cl⁻ or BF₄⁻) [12,13]. The Ru–N–O bond angle was 176.8(4)°, which is compatible with a nitrosonium (NO⁺) character for the NO ligand [12]. The *ina* ligand have two values for the C–O distances in the carboxyl group, 1.323(6) and 1.196(6) Å, which suggests that one of the oxygens in this group is protonated, and therefore the ligand is the isonicotinic acid and not the corresponding anion.

PAMAM dendrimers of generations 0, 2 and 3 have, respectively, 4, 16 and 32 superficial primary amines. Ruthenium complexes were immobilized onto PAMAM via the attachment of dendrimers terminal amines to the carboxyl group of the complex *trans*-[Ru(NO)(NH₃)₄(ina)](BF₄)₃ through an amide bond formation (Fig. 2) [49–51]. Size exclusion chromatography (Sephadex G-25) was used to isolate the products. Two fractions were separated, being the first related to the desired product (G_x/RuNO) and the second, to the excess of *trans*-[Ru(NO)(NH₃)₄(ina)](BF₄)₃.

Two other amidation protocols employing mixed anhydride (treatment with ethyl chloroformate and triethylamine) [50], and another using condensation reagents such as DCC/DMAP (Steglich conditions) failed to give pure products in reasonable yields (less than 10%).

Another synthetic route was tried out without success through the attachment of the isonicotinic acid to dendrimers [49–51] (Fig. 1S, Supplementary material). Then, this product was submitted to the reaction with *trans*-[Ru(NH₃)₄(SO₂)(Cl)]Cl, following the sulfite/sulfate route [12–14]. The problem with this route was the oxidation step of the metal center (Ru²⁺ to Ru³⁺) and of the ligand

Table 2

Selected bond lengths and bond angles for *trans*-[Ru(NO)(NH₃)₄(ina)](BF₄)(SiF₆)-H₂O.

Selected bond lengths (Å)		Selected bond angles (°)	
Ru–N	1.741(4)	Ru–N–O	176.8(4)
O–N	1.132(5)	N–Ru–N(2)	94.23(16)
Ru–N(1)	2.124(3)	N–Ru–N(3)	92.04(16)
Ru–N(2)	2.100(4)	N–Ru–N(4)	89.84(16)
Ru–N(3)	2.116(4)	N–Ru–N(5)	93.15(17)
Ru–N(4)	2.119(4)	N(2)–Ru–N(3)	91.74(15)
Ru–N(5)	2.118(4)	N(3)–Ru–N(4)	87.97(15)
O(11)–C(1)	1.323(6)	N(5)–Ru–N(4)	92.84(15)
O(12)–C(1)	1.196(6)	O(12)–C(1)–O(11)	124.0(4)

(SO₂ to SO₄²⁻) using hydrogen peroxide [12–14,55]. This oxidation step needs to be carried out before the nitric oxide coordination to ruthenium, but it unfortunately compromised the dendrimer structure.

3.2. Spectroscopy

The nitrosyl complexes (attached or not to PAMAM) are EPR silent, indicating that no Ru³⁺ is formed on the anchoring of the complex to dendrimers.

As expected, the ¹H NMR spectra of G_x/RuNO ($x = 0, 2$ and 3) showed similarities to the ¹H NMR spectra of the synthesis precursors: Fig. 3 for G₀/RuNO, and Figs. 2S and 3S (Supplementary material) for G₂/RuNO and G₃/RuNO, respectively. As can be noticed comparing the ¹H NMR spectra of PAMAM G₀ and of G₀/RuNO in Fig. 3, the signals with chemical shift (δ) between 2.7 and 4.0 ppm are related to the dendrimer's moiety of the G₀/RuNO product. This is an indication of the carboxyl attachment (of the *ina* ligand) to the terminal PAMAM amines. The only significant differences between the ¹H NMR spectra of PAMAM (G₀, G₂ and G₃) and G_x/RuNO ($x = 0, 2$ and 3) is the presence of two doublets, centered at $\delta = 8.36$ and 8.75 ppm for the G_x/RuNO species. These signals are also presented in the ¹H NMR spectrum of *trans*-[Ru(NO)(NH₃)₄(ina)]³⁺, with $\delta = 8.36$ and 8.75 ppm (Fig. 4S, Supplementary material), and their presence is consistent with the coordination of the N-heterocyclic ligand to the metal center through the pyridine-type nitrogen [13,14].

An attempt to estimate the number of PAMAM's superficial amines functionalized with the ruthenium complex was carried out through the integration of the hydrogen signals in the ¹H NMR spectra (Fig. 3 and Figs. 2S and 3S; Tables 4S and 5S, Supplementary material). The integrations were performed using the area of the characteristic aromatic hydrogens peaks of the *ina* ligand (which corresponds to four H for each *ina* ligand, Fig. 2) and the area of the aliphatic hydrogens of the PAMAM dendrimers (Fig. 2). These results are summarized in Table 3.

An alternative method to estimate the number of ruthenium nitrosyl attached to PAMAM was performed by analyzing the ruthenium content through ICP-OES (Table 3). The ratio between the theoretical (G_x fully functionalized) and the experimental concentration of ruthenium for a known mass of G_x/RuNO was used as an indication of the degree of the *trans*-[Ru(NO)(NH₃)₄(ina)](BF₄)₃ incorporation on the dendrimer.

According to the ¹H NMR and ICP-OES data, PAMAM G₀ was fully functionalized with *trans*-[Ru(NO)(NH₃)₄(ina)](BF₄)₃, and G₂ and G₃ were functionalized with ~ 8 and ~ 27 ruthenium nitrosyls, respectively. Thus, according to these results, the compounds G₀/RuNO, G₂/RuNO and G₃/RuNO described in this work were able to storage ~ 1.43 , ~ 1.03 and ~ 1.28 $\mu\text{mol NO}$ per mg of compound, respectively. Analogous results were obtained by Benini and collaborators [30], in which PAMAM G₀, G₂ and G₃ were

Table 1
Crystallographic data for *trans*-[Ru(NO)(NH₃)₄(ina)](BF₄)(SiF₆)-H₂O.

Formula	C ₆ H ₁₉ BF ₁₀ N ₆ O ₄ RuSi
Crystal system	monoclinic
Space group	<i>P</i> 2 ₁ / <i>n</i>
<i>a</i> (Å)	7.9616(2)
<i>b</i> (Å)	24.3982(8)
<i>c</i> (Å)	9.9705(3)
α (°)	90
β (°)	98.781(2)
γ (°)	90
<i>V</i> (Å ³)	1914.06(10)
<i>Z</i>	4
Wavelength (Å)	0.71073
ρ_{calc} (Mg m ³)	1.975
<i>R</i> ₁ [<i>I</i> > 2 σ (<i>I</i>)]	0.0473
<i>wR</i> ₂	0.1153
<i>R</i> ₁ (all data)	0.0626
<i>wR</i> ₂ (all data)	0.1246

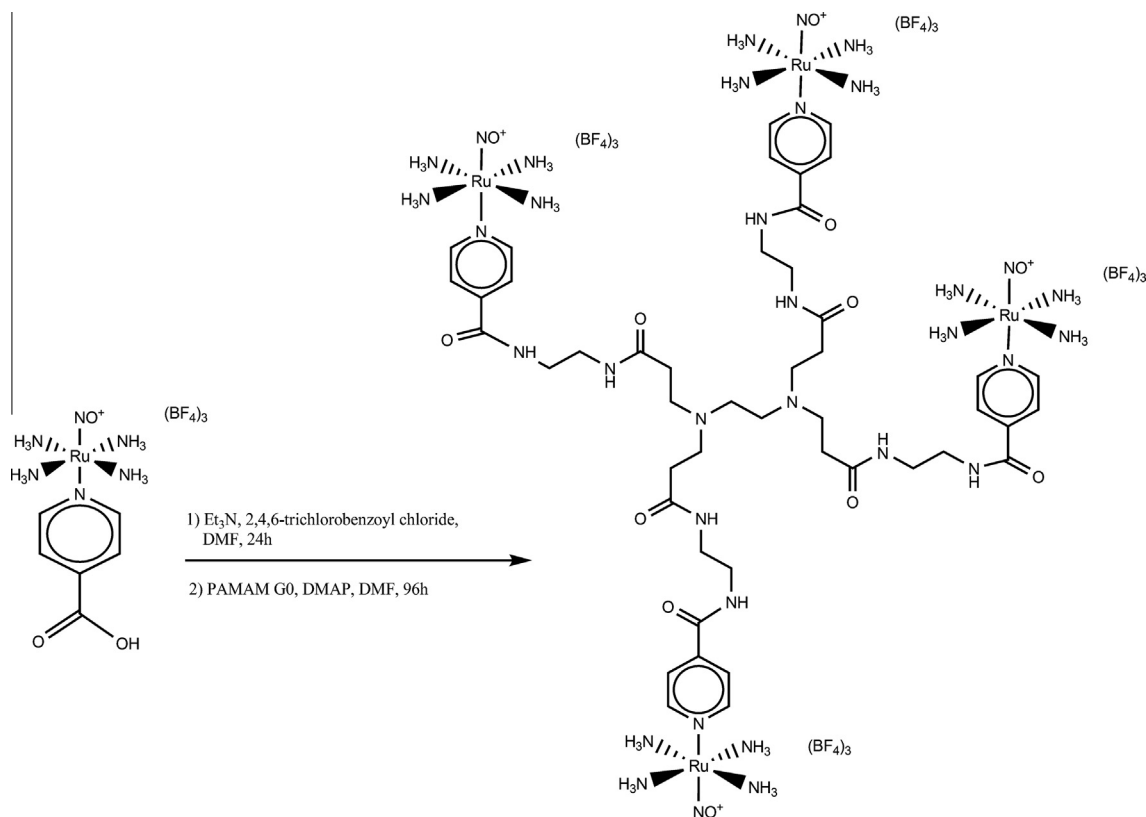


Fig. 2. Functionalization of PAMAM G0 with *trans*-[Ru(NO)(NH₃)₄(ina)](BF₄)₃.

functionalized, respectively, with ~4, ~12 and ~29 [Ru^{III}(edta)(H₂O)]⁻ complexes.

The electronic spectrum of *trans*-[Ru(NO)(NH₃)₄(ina)]³⁺ showed intense bands at 232 nm ($\epsilon = 11.2 \pm 0.3 \times 10^3 \text{ M}^{-1} \text{ cm}^{-1}$) and at 275 nm ($\epsilon = 3.9 \pm 0.2 \times 10^3 \text{ M}^{-1} \text{ cm}^{-1}$), assigned as internal ligand transitions (IL) of *ina*; one band at 335 nm ($\epsilon = 221.9 \pm 7.3 \text{ M}^{-1} \text{ cm}^{-1}$), assigned to Ru d-d transitions, with contributions from a MLCT transition ($d\pi\text{Ru(II)} \rightarrow \pi^*(\text{NO})$), and a weaker band at 466 nm ($\epsilon = 23.9 \pm 6.9 \text{ M}^{-1} \text{ cm}^{-1}$) assigned to $d\pi\text{Ru(II)} \rightarrow \pi^*(\text{NO})$ and $\pi(\text{ina}) \rightarrow \pi^*(\text{NO})$ transitions. These above assignments were tentatively carried out by analogy to previously reported data for other ruthenium tetraammine nitrosyls [12–14]. The UV–Vis spectra of G_x/RuNO ($x = 0, 2$ and 3) exhibited the absorption maxima governed by the ruthenium nitrosyl moiety (Fig. 5S, Supplementary material). These functionalized dendrimers (G_x/RuNO) showed bands at 232, 275, 335 and 466 nm, and the assignments for these bands were similar to the ones described above for *trans*-[Ru(NO)(NH₃)₄(ina)]³⁺. PAMAM G0, G2 and G3 have a band at $\lambda_{\text{max}} = 278 \text{ nm}$ ($\epsilon = 130\text{--}150 \text{ M}^{-1} \text{ cm}^{-1}$). This low intensity band, in comparison to that observed for *trans*-[Ru(NO)(NH₃)₄(ina)]³⁺ in the same region (275 nm, $\epsilon = 3.9 \pm 0.2 \times 10^3 \text{ M}^{-1} \text{ cm}^{-1}$), confirms the small contribution of the dendrimer moiety for the absorption maxima in the UV–Vis spectra of G_x/RuNO products. Similar results were found by Stasko and collaborators [29], which functionalized two PAMAM G4 dendrimers with *S*-nitrosothiol (*N*-acetyl-D,L-penicillamine or *N*-acetyl-L-cysteine), and also by Benini et al. [30].

According to the discussed above, using the ϵ values for $\lambda = 232$ and 275 nm for *trans*-[Ru(NO)(NH₃)₄(ina)](BF₄)₃, would be possible to estimate the number of the PAMAM amines functionalized with the ruthenium nitrosyl complex [30,56]. Thus, assuming that the ϵ values for the G0 functionalized with four *trans*-[Ru(NO)(NH₃)₄(ina)](BF₄)₃, would be in principle approximately four times of that

observed for the free complex [30], the number of functionalized amines was estimated and these results are shown in Table 6S (Supplementary material). Using the same approach was possible to calculate ~8 and ~27 *trans*-[Ru(NO)(NH₃)₄(ina)](BF₄)₃ attached to PAMAM G2 and G3, respectively. These results are consistent with the ones calculated from NMR and ICP-OES data (Table 3). Nevertheless, the approach using only UV–Vis is not conclusive and must be performed together with other techniques (as ¹H NMR and ruthenium analysis) in order to obtain a more reliable value.

The formal reduction potentials of the Ru^{II}NO⁺/Ru^{II}NO⁰ couple ($E_{\text{NO}^+/\text{NO}^0}$) for *trans*-[Ru(NO)(NH₃)₄(ina)]³⁺ and for G_x/RuNO ($x = 0, 2$ and 3) in solution, were similar, ~60 mV versus NHE (Table 4). Analogous results were obtained for other ruthenium nitrosyl immobilized on PAMAM dendrimers [30] and in other matrices [17]. It is interesting to recall that these potentials are in the accessible range for biological reducing agents [7,57], which potentially enables the title compounds as candidates for therapy use.

The $\nu(\text{NO}^+)$ frequencies for the complex *trans*-[Ru(NO)(NH₃)₄(ina)](BF₄)₃ (attached or not to PAMAM) are also presented in Table 4. All the ruthenium compounds described in this work showed a medium to strong intensity band in the 1930–1933 cm⁻¹ range ascribed to $\nu(\text{NO}^+)$ (Figs. 6S–8S, Supplementary material), which is compatible with a nitrosonium (NO⁺) character of the NO ligand (as previously discussed in the crystallographic results in the Section 3.1) [12]. Comparing the FT-IR spectra of the products (G_x/RuNO) with the starting compounds is also possible to notice the appearance of a medium intensity band in the region of 1640–1680 cm⁻¹ for G_x/RuNO ($x = 0, 2$ and 3), assigned to the amide I (νCO) [30,42,58], which is present on PAMAM (G0, G2 and G3) but is absent in the complex *trans*-[Ru(NO)(NH₃)₄(ina)](BF₄)₃ (Figs. 6S–8S, Supplementary material). This is an indicative of the amide bond formed between the *ina* ligand and the dendrimer. Other differences observed in the FT-IR spectra of G_x/

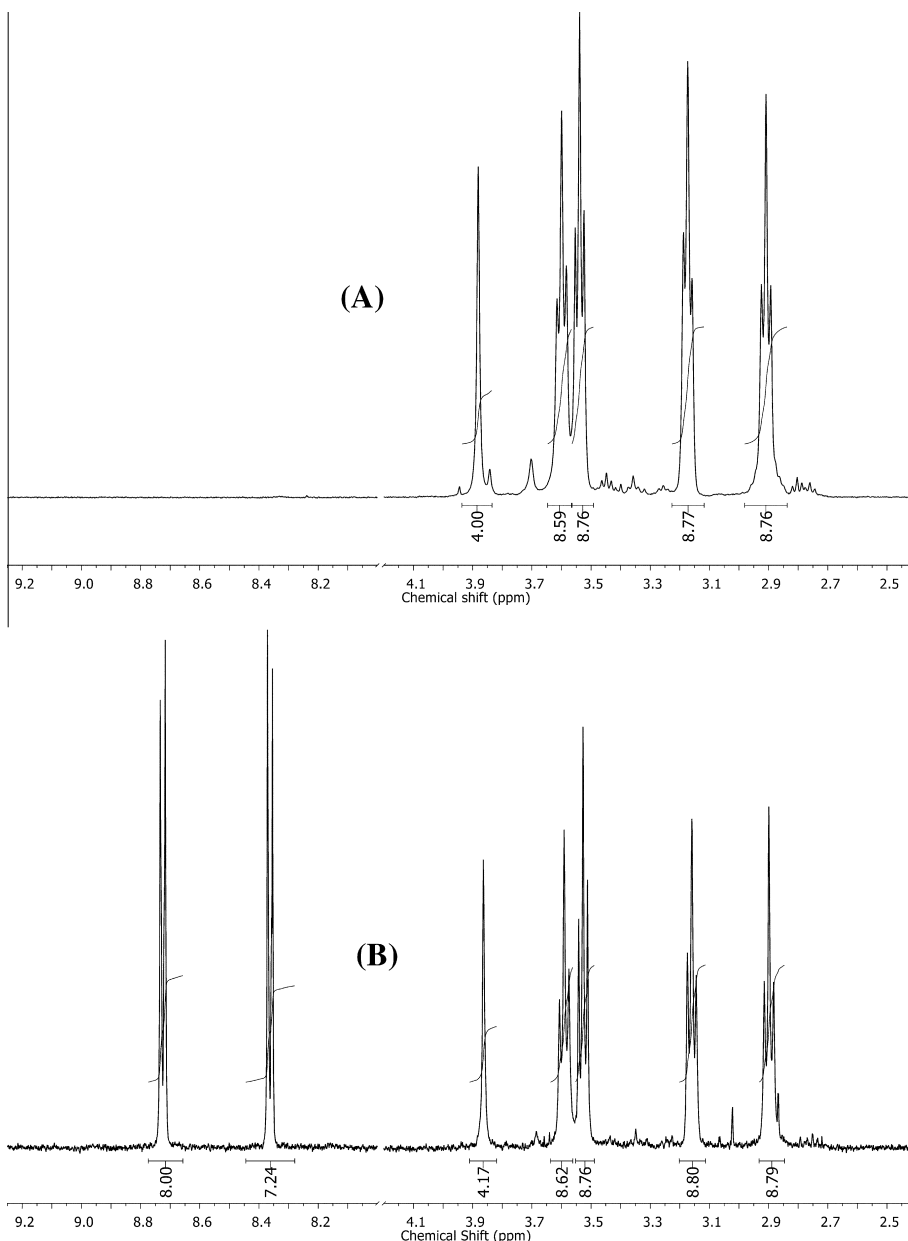


Fig. 3. ^1H NMR spectra of (A) PAMAM G0 and (B) G0/RuNO (1.0 mol L $^{-1}$ CF $_3$ COOD in D $_2$ O).

Table 3

Estimative of the PAMAM's superficial amines functionalized with *trans*-[Ru(NO)(NH $_3$) $_4$ (ina)](BF $_4$) $_3$ performed by ^1H NMR and ICP-OES.

Compounds	Number of PAMAM's superficial amines ^a	Number of functionalized amines	
		^1H NMR	ICP-OES ^b
G0/RuNO	4	4	3.7 ± 0.21
G2/RuNO	16	7.7	7.3 ± 0.65
G3/RuNO	32	28.1	26.3 ± 0.83

^a Superficial amines of PAMAM G0, G2 and G3

^b Results from three independent assays.

RuNO in relation to that of *trans*-[Ru(NO)(NH $_3$) $_4$ (ina)](BF $_4$) $_3$ are the appearance of strong broad bands around 3070–3080 cm $^{-1}$ (ν (NH)) and 2940–2960 cm $^{-1}$ (ν (NH) and ν (CH)) [42] for Gx/RuNO, which are present in PAMAM (G0, G2 and G3) dendrimers [58] in the same region (Figs. 6S–8S, Supplementary material) and are absent in the FT-IR spectrum of *trans*-[Ru(NO)(NH $_3$) $_4$ (ina)](BF $_4$) $_3$.

Thus, the electrochemical (DPV and CV) and spectroscopic (UV–Vis and FT-IR) results suggest that the functionalization of

dendrimers with *trans*-[Ru(NO)(NH $_3$) $_4$ (ina)](BF $_4$) $_3$ did not significantly alter the spectroscopic and electrochemical characteristics of the ruthenium complex.

3.3. Photochemical NO release

NO release from ruthenium tetraammine nitrosyl (Eq. (1)) can be achieved by irradiation of these complexes in solution with light

Table 4

Electrochemical data and $\nu(\text{NO})$ frequencies for ruthenium nitrosyl complexes attached or not to PAMAM dendrimer.

Compound	$E_{\text{cp}}(\text{NO}^+/\text{NO}^0)$ (mV vs. NHE) ^a	$\nu(\text{NO}^+)(\text{cm}^{-1})^b$
<i>trans</i> - [Ru(NO)(NH ₃) ₄ (ina)](BF ₄) ₃	59	1933
G0/RuNO	57	1931
G2/RuNO	58	1930
G3/RuNO	59	1931

^a Potential of the cathodic peak obtained by differential pulse voltammetry, pH 2.0, $\mu = 0.10 \text{ M}$ (CF₃COOH/CF₃COONa), $T = (25 \pm 1)^\circ\text{C}$; scan rate = 5 mV/s, pulse height = 50 mV.

^b KBr pellet, resolution of 4 cm⁻¹.

in the range of 300–370 nm [15]. Thus, solutions containing *trans*-[Ru(NO)(NH₃)₄(ina)]³⁺ (attached or not to PAMAM G2) were irradiated at 355 nm in phosphate buffer (pH 7.4) in the presence of PTIO. This last compound is a well known nitric oxide spin trap [52,53]. PTIO reacts with NO yielding PTI, as illustrated in Fig. 4. Both PTIO and PTI are paramagnetic species, and therefore can be detected and distinguished through EPR spectroscopy [52,53]. Thus, performing the photochemical reaction for *trans*-[Ru(NO)(NH₃)₄(ina)]³⁺ and for G2/RuNO in the presence of PTIO, it was possible to detect the NO release from these compounds due to the observation of the signals related to the PTI species (Fig. 5) [52,53]. The values obtained for the hyperfine splitting constant (Fig. 5) were: $a_{\text{N}}^{1,3} = 0.82 \text{ mT}$ for PTIO; $a_{\text{N}}^1 = 0.98 \text{ mT}$ and $a_{\text{N}}^3 = 0.44 \text{ mT}$ for PTI, which are consistent with the ones reported previously [52].

This photochemical reaction was also performed for *trans*-[Ru(NO)(NH₃)₄(ina)]³⁺ and for G3/RuNO, in the absence of PTIO, in aqueous solution (pH 2.0, $\mu = 0.10 \text{ mol L}^{-1}$ CF₃COOH/CF₃COONa), and it was monitored through UV–Vis spectroscopy (Fig. 9S, Supplementary material). It was possible to observe an absorbance decrease at $\sim 230 \text{ nm}$ concomitant with an absorbance increase at 275 nm and at 300–350 nm. Also an isosbestic point was observed at 249 nm. This photochemical behavior for the nitrosyl complex (attached or not to PAMAM) was similar to that previously described for other ruthenium tetraammine nitrosyls in solution [15] or immobilized in different matrices [17,22]. The formation of the *trans*-[Ru^{III}(NH₃)₄(H₂O)(ina)]³⁺ photoproduct [15] (pH 2.0, $\mu = 0.10 \text{ mol L}^{-1}$, CF₃COOH/CF₃COONa) was confirmed through EPR spectroscopy (Fig. 6) [12,14,15].

The *g*-factor for *trans*-[Ru^{III}(NH₃)₄(H₂O)(ina)]³⁺ (not attached to PAMAM) is $g = 2.543$, and for *trans*-[Ru^{III}(NH₃)₄(H₂O)(ina)]³⁺ attached to PAMAM G3 are $g_{\perp} = 2.481$ and $g_{\parallel} = 2.675$. The other *g*-factor for *trans*-[Ru^{III}(NH₃)₄(H₂O)(ina)]³⁺ (not attached to PAMAM) was not observed and this difficulty was previously reported and thoroughly discussed elsewhere [55,59]. Also, when comparing the EPR spectra for *trans*-[Ru^{III}(NH₃)₄(H₂O)(ina)]³⁺ attached or not to PAMAM (Fig. 6), a shoulder can be observed in the G3/RuNO spectrum. This was tentatively attributed to matrix effects [17].

Furthermore, as far as the compounds described in this work are concerned, the photochemical NO release activation pathway requires light excitation in a non favorable region of the spectra ($\lambda \leq 400 \text{ nm}$). Thus some coordination sphere tailoring is necessary

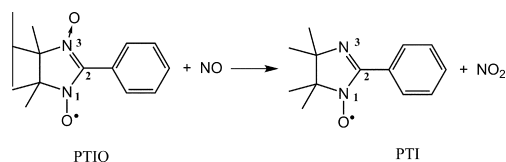


Fig. 4. PTIO conversion into PTI through the reaction with NO [53, 54].

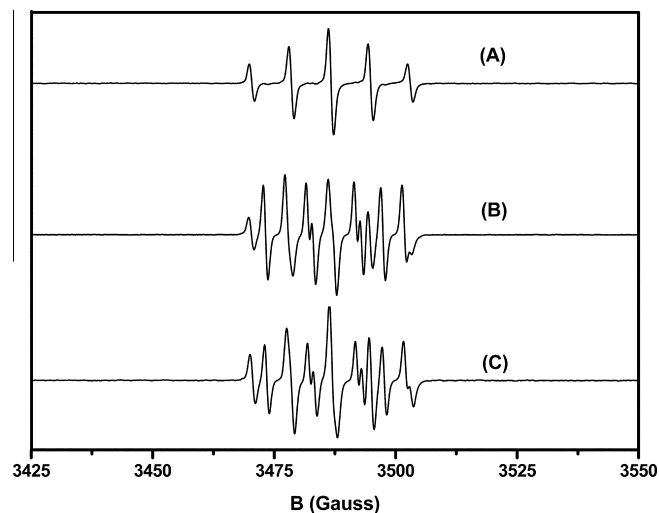
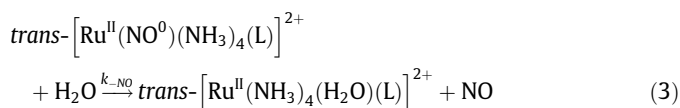
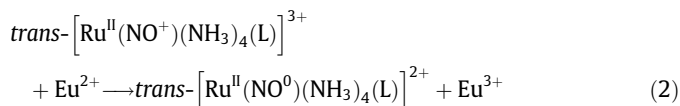


Fig. 5. EPR detection of NO release from the ruthenium nitrosyl upon photochemical reaction. EPR spectra of irradiated solutions containing: (A) only PTIO (control), irradiated for 10 min; (B) PTIO + *trans*-[Ru(NO)(NH₃)₄(ina)]³⁺ and (C) PTIO + G2/RuNO, both irradiated for 5 min. (phosphate buffer solutions pH 7.4; $C_{\text{Ru}} = 7.5 \times 10^{-4} \text{ mol L}^{-1}$, $C_{\text{PTIO}} = 7.5 \times 10^{-4} \text{ mol L}^{-1}$; $\lambda_{\text{irr}} = 355 \text{ nm}$, $\sim 2 \text{ mJ/pulse}$; $T = 25 \pm 1^\circ\text{C}$).

to achieve a more accessible irradiation region to be used in photodynamic therapy.

3.4. NO release from chemical reduction

It is well established that the NO dissociation from *trans*-[Ru(NO)(NH₃)₄(L)]³⁺ complexes can be triggered by the reaction with Eu²⁺ ions [12–14], as shown in Eqs. (2) and (3).



Thus, the NO dissociation from ruthenium nitrosyl attached to PAMAM was similarly investigated through the reaction with Eu²⁺ ions. As observed in Fig. 7, the DPV of a solution containing G3/RuNO showed a cathodic peak (E_{cp1}) at $\sim 0.060 \text{ V}$ versus NHE, ascribed to the RuNO⁺/RuNO⁰ process. After the reaction of G3/RuNO with Eu²⁺, the process described above disappeared, whereas a new one was observed with $E_{\text{ap1}} \sim 0.295 \text{ V}$ versus NHE, which was assigned to the [RuH₂O]³⁺/[RuH₂O]²⁺ couple in *trans*-[Ru(NH₃)₄(H₂O)(ina)]²⁺ (Fig. 7). Also, an electrochemical anodic wave with $E_{\text{ap2}} \sim 0.753 \text{ V}$ versus NHE can be observed. This last electrochemical process is due to the oxidation of free NO in solution [14,60], confirming that the NO was released from G3/RuNO after the reaction with Eu²⁺.

The reaction between Gx/RuNO and Eu²⁺ was also investigated spectrophotometrically, as shown in the Fig. 8 for G3/RuNO. After the addition of Eu²⁺ to the solution containing G3/RuNO, a new band at 492 nm appeared, consistent with the *trans*-[Ru(NH₃)₄(H₂O)(ina)]²⁺ formation, and which was assigned to a metal to ligand charge transfer (MLCT) $d\pi(\text{Ru}) \rightarrow \pi^*(\text{ina})$ [12–14].

Therefore, as suggested by DPV and electronic spectroscopy data, the ions *trans*-[Ru(NO)(NH₃)₄(ina)]³⁺ attached to PAMAM, after reduction, exhibited nitric oxide dissociation and the respective formation of the aqua species *trans*-[Ru(NH₃)₄(H₂O)(ina)]²⁺.

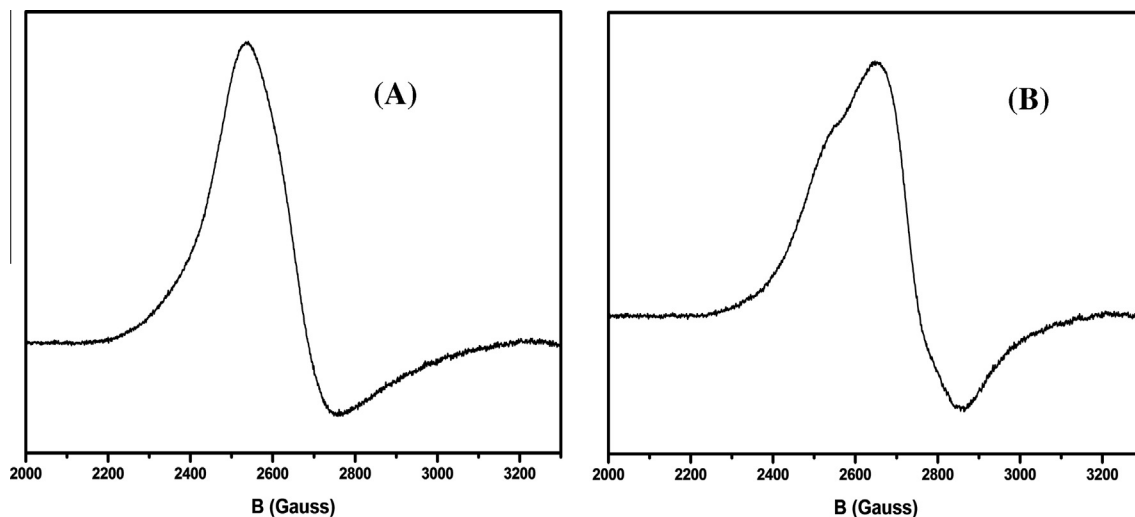


Fig. 6. EPR spectra of solutions containing (A) *trans*-[Ru(NO)(NH₃)₄(ina)]³⁺ and (B) G3/RuNO after 30 min of laser irradiation ($C_{\text{Ru}} \sim 2.0 \times 10^{-3} \text{ mol L}^{-1}$; pH 2.0, $\mu = 0.10 \text{ mol L}^{-1} \text{ CF}_3\text{COOH/CF}_3\text{COONa}$; $\lambda_{\text{irr}} = 355 \text{ nm}$, $\sim 2 \text{ mJ/pulse}$; $T = 25 \pm 1 \text{ }^\circ\text{C}$). EPR spectra were recorded at $T = 77 \text{ K}$.

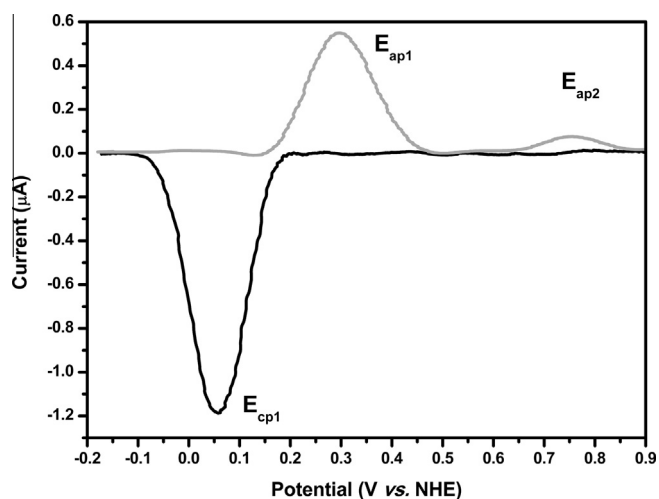


Fig. 7. Differential pulse voltammograms of the reaction between G3/RuNO and Eu²⁺. DPV of G3/RuNO before (black line) and after (gray line) the reaction with Eu²⁺. ($C_{\text{Ru}} = 5.0 \times 10^{-4} \text{ mol L}^{-1}$; $C_{\text{Eu}^{2+}} = 2.0 \times 10^{-3} \text{ mol L}^{-1}$; pH 2.0, $\mu = 0.10 \text{ mol L}^{-1} \text{ CF}_3\text{COOH/CF}_3\text{COONa}$; scan rate = 5 mV/s; pulse height = 50 mV; $T = 25 \pm 1 \text{ }^\circ\text{C}$).

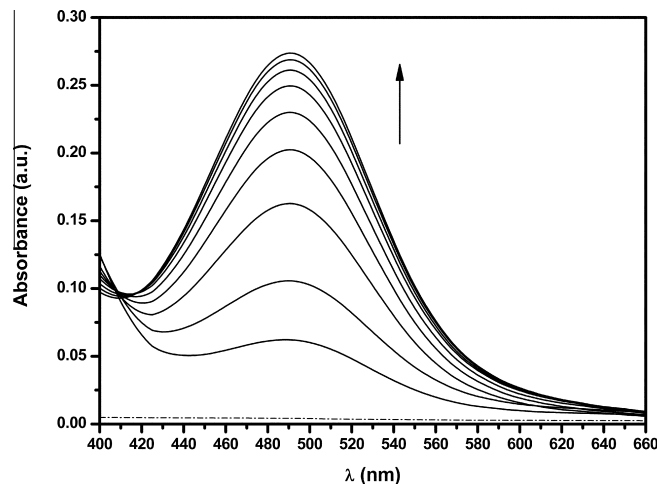


Fig. 8. Spectral changes during the reaction between G3/RuNO and Eu²⁺. Initial spectrum of G3/RuNO (dashed line). The first spectrum was recorded 30s after the addition of Eu²⁺ to the solution containing G3/RuNO, and the next ones, every 1 min ($C_{\text{Ru}} = 6.5 \times 10^{-5} \text{ mol L}^{-1}$; $C_{\text{Eu}^{2+}} = 2.6 \times 10^{-4} \text{ mol L}^{-1}$; pH 2.0, $\mu = 0.10 \text{ mol L}^{-1} \text{ CF}_3\text{COOH/CF}_3\text{COONa}$; $T = 25 \pm 1 \text{ }^\circ\text{C}$).

Toledo *et al.* [57] found a correlation between the rate constant for NO dissociation ($k_{-\text{NO}}$), represented in Eq. (3), and the sum of the electrochemical parameters ($\sum E_L$), introduced by Lever [61], as shown in Eq. (4):

$$K_{-\text{NO}} = (-0.81 \times \sum E_L) + 0.48; \text{ (with } R = 0.997) \quad (4)$$

Using this correlation (with $\sum E_L = 0.57$) [57,61], it was possible to estimate the rate constant for the NO dissociation from *trans*-[Ru(NO)(NH₃)₄(ina)]²⁺ as $k_{-\text{NO}} \sim 0.0183 \text{ s}^{-1}$, with $t_{1/2} \sim 38 \text{ s}$. Since no drastic changes were observed between the ruthenium nitrosyl properties in solution or attached to dendrimers [30] it is likely that the $k_{-\text{NO}}$ for Gx/RuNO would be around 0.02 s^{-1} [30].

The NO release mechanism for the NO-releasing dendrimers described in the literature [18–20,29,30,62] is diversified. Dendrimers functionalized with *N*-diazoniumdiolates [18–20] release NO spontaneously in physiological conditions with a $t_{1/2}$ for NO release varying from 1.4–293 min, depending on the dendrimers surface modifications [18,20,62]. Dendrimers functionalized with

S-nitrosothiols [29] release NO by two main pathways: photo-initiated decomposition, with $t_{1/2}$ in the range of 34–200 min, and transition metal-mediated catalytic decomposition (based on Cu⁺/Cu²⁺ redox couple) with $t_{1/2}$ in the range of 1.5–106 min [29]. PAMAM functionalized with [Ru(edta)(NO)]⁻ [30] release NO in an analogous way to that observed for the compounds described in this work (by chemical reduction) with $t_{1/2}$ in the range of 4–8 min.

Since the NO liberation from ruthenium nitrosyl compounds can be triggered on a controlled way by photochemical and thermal activation (reduction), these compounds offer the possibility of designing and exploring them as new platforms for NO transport.

Therefore, when dealing with hypoxic conditions, as in the infections like Chaga's Disease and Leishmaniasis, or even in solid tumors, the environment might provide the necessary reducers for the Ru^{II}NO⁺/Ru^{II}NO⁰ reduction in the nitrosyl compounds. Thus, Gx/RuNO could be good candidates to be used in these therapies.

Indeed, some preliminary experiments (*in vitro*) have been carried out with the compounds Gx/RuNO against *Trypanosoma cruzi* (Y strain). Results collected to date indicate that the trypanocidal activity of G0/RuNO and G2/RuNO ($C_{Ru} = 200 \times 10^{-6} \text{ mol L}^{-1}$) were approximately 82% and 88%, respectively. These compounds exhibited a trypanocidal activity slightly higher than that observed for the complex *trans*-[Ru(NO)(NH₃)₄(ina)](BF₄)₃ (72% of trypanocidal activity for $C_{Ru} = 200 \times 10^{-6} \text{ mol L}^{-1}$). The *in vivo* experiments, in which these differences might be more evident, are in course and these results will be reported later on.

4. Conclusion

The functionalization of PAMAM dendrimers with *trans*-[Ru(NO)(NH₃)₄(ina)]³⁺ complexes was performed in one-step synthesis. As far as the data collected are concerned, no significant changes in the chemical and photochemical properties of the ruthenium nitrosyl complex occurs with its attachment to the dendrimers. The Gx/RuNO compounds are robust and able to store a high payload of nitric oxide, which can be released on a controlled way when triggered by light irradiation or by chemical reduction.

Acknowledgments

The authors acknowledge the Brazilian agencies FAPESP, CAPES and CNPq for their financial support.

Appendix A. Supplementary data

Supplementary data associated with this article can be found, in the online version, at <http://dx.doi.org/10.1016/j.ica.2013.07.009>.

References

- [1] J.M. Fukuto, S.J. Carrington, D.J. Tantillo, J.G. Harrison, L.J. Ignarro, B.A. Freeman, A. Chen, D.A. Wink, *Chem. Res. Toxicol.* 25 (2012) 769.
- [2] J.C. Toledo Jr., O. Augusto, *Chem. Res. Toxicol.* 25 (2012) 975.
- [3] S. Moncada, R.M.J. Palmer, E.A. Higgs, *Pharmacol. Rev.* 43 (1991) 109.
- [4] M.R. Miller, I.L. Megson, *Br. J. Pharmacol.* 151 (2007) 305.
- [5] R.A.M. Serafim, M.C. Primi, G.H.G. Trossini, E.I. Ferreira, *Curr. Med. Chem.* 19 (2012) 386.
- [6] P.G. Wang, M. Xian, X. Tang, X. Wu, Z. Wen, T. Cai, A.J. Janczuk, *Chem. Rev.* 102 (2002) 1091.
- [7] J.J. Silva, A.L. Osakabe, W.R. Pavanelli, J.S. Silva, D.W. Franco, *Br. J. Pharmacol.* 152 (2007) 112.
- [8] J.J. Silva, W.R. Pavanelli, J.C. Pereira, J.S. Silva, D.W. Franco, *Antimicrob. Agents Chemother.* 53 (2009) 4414.
- [9] J.C. Pereira, V. Carregaro, D.L. Costa, J.S. Silva, F.Q. Cunha, D.W. Franco, *Eur. J. Med. Chem.* 45 (2010) 4180.
- [10] L.K. Keefer, *ACS Chem. Biol.* 6 (2011) 1147.
- [11] R.Z. Osti, F.A. Serrano, T. Paschoalin, M.H.S. Massaoka, L.R. Travassos, D.R. Truzzi, E.G. Rodrigues, D.W. Franco, *Aust. J. Chem.* 65 (2012) 1333.
- [12] E. Tfouni, M. Krieger, B.R. McGarvey, D.W. Franco, *Coord. Chem. Rev.* 236 (2003) 57.
- [13] S.S.S. Borges, C.U. Davanzo, E.E. Castellano, J. Z-Schpector, S.C. Silva, D.W. Franco, *Inorg. Chem.* 37 (1998) 2670.
- [14] M.G. Gomes, C.U. Davanzo, S.C. Silva, L.G.F. Lopes, P.S. Santos, D.W. Franco, *J. Chem. Soc., Dalton Trans.* (1998) 601.
- [15] R.M. Carlos, A.A. Ferro, H.A.S. Silva, M.G. Gomes, S.S.S. Borges, P.C. Ford, E. Tfouni, D.W. Franco, *Inorg. Chim. Acta* 357 (2004) 1381.
- [16] A.A. Eroy-Reveles, P.K. Mascharak, *Med. Chem.* 1 (2009) 1497.
- [17] E. Tfouni, F.G. Doro, A.J. Gomes, R.S. Silva, G. Metzker, *Coord. Chem. Rev.* 254 (2010) 355.
- [18] N.A. Stasko, M.H. Schoenfish, *J. Am. Chem. Soc.* 128 (2006) 8265.
- [19] L.J. Taitte, J.L. West, *J. Biomater. Sci., Polym. Ed.* 17 (2006) 1159.
- [20] Y. Lu, B. Sun, C. Li, M.H. Schoenfish, *Chem. Mater.* 23 (2011) 4227.
- [21] P.G. Zanichelli, R.L. Sernaglia, D.W. Franco, *Langmuir* 22 (2006) 203.
- [22] F.G. Doro, U.P. Rodrigues-Filho, E. Tfouni, *J. Colloid Interface Sci.* 307 (2007) 405.
- [23] J. Bordini, P.C. Ford, E. Tfouni, *Chem. Commun.* (2005) 4169.
- [24] K.Q. Ferreira, J.F. Schneider, P.A.P. Nascente, U.P. Rodrigues, E. Tfouni, *J. Colloid Interface Sci.* 300 (2006) 543.
- [25] D.A. Riccio, K.P. Dobmeier, E.M. Hetrick, B.J. Privett, H.S. Paul, M.H. Schoenfish, *Biomaterials* 30 (2009) 4494.
- [26] J.J. Koehler, J. Zhao, S.S. Jedlicka, D.M. Porterfield, J.L. Rickus, *J. Phys. Chem. B* 112 (2008) 15086.
- [27] S.L. Huang, P.H. Kee, H. Kim, M.R. Moody, S.M. Chrzanowski, R.C. MacDonald, D.D. McPherson, *J. Am. Coll. Cardiol.* 54 (2009) 652.
- [28] M. Barone, M.T. Sciortino, D. Zaccaria, A. Mazzaglia, S. Sortino, *J. Mater. Chem.* 18 (2008) 5531.
- [29] N.A. Stasko, T.H. Fischer, M.H. Schoenfish, *Biomacromolecules* 9 (2008) 834.
- [30] P.G.Z. Benini, B.R. McGarvey, D.W. Franco, *Nitric Oxide* 19 (2008) 245.
- [31] A.B. Seabra, N. Durán, *J. Mater. Chem.* 20 (2010) 1624.
- [32] S. Hong, P.R. Leroueil, I.J. Majoros, B.G. Orr, J.R. Baker Jr., M.M.B. Holl, *Chem. Biol.* 14 (2007) 107.
- [33] J.H. Myung, K.A. Gajjar, J. Saric, D.T. Eddington, S. Hong, *Angew. Chem., Int. Ed.* 50 (2011) 1.
- [34] E.R. Gillies, J.M.J. Fréchet, *Drug Discov. Today* 10 (2005) 35.
- [35] S.H. Medina, M.E.H. El-Sayed, *Chem. Rev. (Washington, DC, US)* 109 (2009) 3141.
- [36] W. Wijagkanalan, S. Kawakami, M. Hashida, *Pharm. Res.* 28 (2011) 1500.
- [37] R. Jevprasesphant, J. Penny, R. Jalal, D. Attwood, N.B. McKeownb, A. D'Emanuele, *Int. J. Pharm. (Amsterdam, Neth.)* 252 (2003) 263.
- [38] M. Ciolkowski, J.F. Petersen, M. Ficker, A. Janaszewska, J.B. Christensen, B. Klajnert, M. Bryszewska, *Nanomedicine* 8 (2012) 815.
- [39] S. Sadekar, H. Ghandehari, *Adv. Drug Delivery Rev.* 64 (2012) 571.
- [40] D.F. Shriver, *The Manipulation of Air-Sensitive Compound*, McGraw-Hill, New York, 1969.
- [41] M. Biancardo, P.F.H. Schwab, R. Argazzi, C.A. Bignozzi, *Inorg. Chem.* 42 (2003) 3966.
- [42] K. Nakamoto, *Infrared and Raman Spectra of Inorganic and Coordination Compounds*, John Wiley and Sons, New York, 1978.
- [43] COLLECT, Enraf-Nonius, Nonius BV, Delft, The Netherlands, 1997–2000.
- [44] Z. Otwinowski, W. Minor, H.K.L. Denzo, *Methods in Enzymology*, New York, vol. 276, Academic Press, New York, 1997.
- [45] P. Coppens, L. Leiserow, D. Rabinovi, *Acta Crystallogr.* 18 (1965) 1035.
- [46] G.M. Sheldrick, SHELXS97, Program for Crystal Structure Refinement, University of Göttingen, Göttingen, Germany, 1997.
- [47] G.M. Sheldrick, SHELXS97, Program for Crystal Structure Analysis, University of Göttingen, Göttingen, Germany, 1997.
- [48] L.J. Farrugia, *J. Appl. Crystallogr.* 30 (1997) 565.
- [49] J. Inanaga, K. Hirata, H. Saki, T. Katsuki, M. Yamaguchi, *Bull. Chem. Soc. Jpn.* 52 (1979) 1989.
- [50] R. Schobert, B. Biersack, *Inorg. Chim. Acta* 358 (2005) 3369.
- [51] R. Schobert, S. Seibt, K. Effenberger-Neidnicht, C. Underhill, B. Biersack, G.L. Hammond, *Steroids* 76 (2011) 393.
- [52] T. Akaike, M. Yoshida, Y. Miyamoto, K. Sato, M. Kohno, K. Sasamoto, K. Miyazaki, S. Ueda, H. Maeda, *Biochemistry* 32 (1993) 827.
- [53] N. Hogg, *Free Radical Biol. Med.* 49 (2010) 122.
- [54] F. Bottomley, *J. Chem. Soc., Dalton Trans.* (1974) 1600.
- [55] H.A.S. Silva, B.R. McGarvey, R.H.A. Santos, M. Bertotti, V. Mori, D.W. Franco, *Can. J. Chem.* 79 (2001) 679.
- [56] M. Martín-Zarco, S. Toribio, J.C. García-Martínez, J. Rodríguez-López, *J. Polym. Sci., Part A* 47 (2009) 6409.
- [57] J.C. Toledo, H.A.S. Silva, M. Scarpellini, V. Mori, A.J. Camargo, M. Bertotti, D.W. Franco, *Eur. J. Inorg. Chem.* 9 (2004) 1879.
- [58] A. Manna, T. Imae, K. Aoi, M. Okada, T. Yogo, *Chem. Mater.* 13 (2001) 1674.
- [59] B.R. McGarvey, N.C. Batista, C.W.B. Bezerra, M.S. Schultz, D.W. Franco, *Inorg. Chem.* 37 (1998) 2865.
- [60] V. Mori, M. Bertotti, *Analyst* 125 (2000) 1629.
- [61] A.B.P. Lever, *Inorg. Chem.* 29 (1990) 1271.
- [62] A.C. Roveda Jr., D.W. Franco, *Braz. J. Pharm. Sci.* 49 (2013). (in press, Accepted Manuscript).